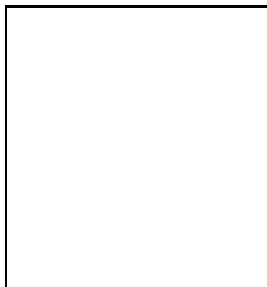# HIGH SENSITIVITY ANTI-NEUTRINO DETECTION BY KAMLAND

S. HATAKEYAMA

on behalf of the KamLAND Collaboration

Department of Physics and Astronomy, Louisiana State University,
Baton Rouge, Louisiana 70803, USA

Electron anti-neutrinos ($\bar{\nu}_e$) from nuclear power reactors have been observed by KamLAND. Data from 0.16 kton·year exposure (145.1 live days) indicates disappearance of $\bar{\nu}_e$ at 99.95% C.L. in the energy range 2.6 MeV $< E_{\bar{\nu}_e} <$ 8.0 MeV. Considering two-flavor neutrino oscillation with CPT invariance, the only remaining solution to the solar neutrino problem is the Large Mixing Angle (LMA) solution. In addition a 0.28kton·year exposure (185.5 live days) was searched for $\bar{\nu}_e$ in the energy range 8.3 MeV $< E_{\bar{\nu}_e} <$ 14.8 MeV. No candidate events were found with expected background of 1.1±0.4 events. Assuming that the origin of $\bar{\nu}_e$ in this energy region comes from ^{8}B solar ν_e, we find an upper limit of ν_e to $\bar{\nu}_e$ conversion probability of 2.8 $\times 10^{-4}$.

1 KamLAND Experiment

1.1 Motivation of the Experiment

Kamioka Liquid scintillator Anti-Neutrino Detector (KamLAND) started operation on January 21st 2002. The observation of $\bar{\nu}_e$'s from nuclear power reactors was the primary object of the KamLAND experiment because it was expected to solve the solar neutrino problem and set a strong constraint on the neutrino oscillation parameters. The search for solar anti-neutrinos was undertaken to examine two types of theoretical framework, spin-flavor precession and neutrino decay. This letter describes the reactor $\bar{\nu}_e$ observation [1] and the solar $\bar{\nu}_e$ search.[2] KamLAND may also observe other neutrino sources. The observation of geo-neutrinos in high statistics will reveal quantitative information of U and Th in the earth. Observation of ^{7}Be solar neutrinos will be the next goal of KamLAND, however we still need to purify the liquid scintilator to achieve a detection of the ^{7}Be neutrino signal. Other possible neutrino sources, such as supernova neutrinos and relic neutrinos are also an exciting prospect. KamLAND also has the ability to detect nucleon decay.

1.2 Detector Overview

KamLAND is located 1000 m under ground in the Kamioka mine in Japan. The detector is composed of a sphere shaped inner detector (ID) and a cylindrical shaped outer detector (OD). The inner detector which consists of 1200 m^3 of liquid scintillator (LS) (90% dodecane, 20% pseudocumene and 1.52 g/l of PPO) is contained within a 13 m diameter balloon (134 μm thick transparent nylon/EVOH composite film) which sits inside 1800 m^3 of buffer oil (50% dodecane, 50% isoparaffin). On the inside edge of ID sphere 1325 fast timing 17 inch diameter PMTs and 554 20 inch diameter PMTs collect photons from the LS. Only the 17 inch PMTs were used for

this analysis. The photo coverage was about 22%. The OD is filled with purified water and is instrumented with 225 20 inch diameter PMTs. The OD is a water cherenkov detector used to eliminate cosmic ray muons. It also acts as a shield against radioactivity from the surrounding rock. KamLAND is now stable and taking data 24 hours/days except for calibration runs or unexpected shutdowns. The average trigger rate is $\sim$ 30Hz with the primary trigger threshold (200 PMT hits, $\sim$0.7MeV).

1.3 Energy and Vertex Calibration

To calibrate the energy scale from 1MeV to several MeV, various radioactive sources are deployed along vertical-axis of detector. The sources are ^{68}Ge (1.012MeV $\gamma + \gamma$), ^{60}Co (2.506MeV $\gamma + \gamma$), ^{65}Zn (1.116MeV γ) and ^{241}Am/Be (2.20, 4.40, 7.6MeV γ). We also use γ-rays from neutron capture on proton (2.2MeV) and neutron capture on ^{12}C (4.95MeV). These neutrons are generated by spallation from the passage of cosmic-ray muons in the LS. The estimated energy resolution is about $7.5\%/\sqrt{E(\mathrm{MeV})}$. Light yield is 300 p.e./MeV. Radioactive sources are also used to obtain the positioning bias of the vertex reconstruction. The bias of the reconstructed vertex position was less than $\pm$5cm along z-axis within the fiducial volume.

1.4 Detection of $\bar{\nu}_e$ by Delayed Coincidence

Electron anti-neutrino is detected using the inverse β decay reaction in the LS,

$$\bar{\nu}_e + p \rightarrow e^+ + n. \tag{1}$$

The generated positron is immediately annihilated to 2 γ generating a prompt signal. On the other hand the neutron is thermalized in the LS and captured on a proton after $\sim$200 μs, generating a 2.2 MeV γ as a delayed signal. By requiring the coincidence of prompt and delayed signal, background can be reduced dramatically. The visible energy of prompt signal is related to the $\bar{\nu}_e$ energy by:

$$
\begin{aligned}
E_{\mathrm{vis}} &= E_{\bar{\nu}_e} - (\Delta m_{np} + m_e) - T_n(\theta) + 2m_e & (2) \\
&= E_{\bar{\nu}_e} - 0.782\mathrm{MeV} - T_n(\theta) & (3)
\end{aligned}
$$

where $E_{\bar{\nu}_e}$ is energy of the $\bar{\nu}_e$, Δm_{np} is the mass difference between the neutron and proton, m_e is the electron mass and $T_n(\theta)$ is the kinetic energy of the neutron scattered by an angle θ. The detection efficiency for inverse β decay events is estimated from Monte Carlo simulation and calibration data to be $84.2 \pm 1.5\%$. The main contributions to the detection inefficiency are the cuts on the distance between the prompt and delayed vertices ($89.8 \pm 1.6\%$), the time between the prompt and delayed vertices ($95.3 \pm 0.3\%$), neutron capture on protons (99.5%), and the energy of the delayed event ($98.9 \pm 0.1\%$).

1.5 Spallation Events after Muon

Although KamLAND is located deep underground (2700 m water equivalent), muons originating from cosmic-rays pass through the detector at a frequency of 0.34Hz. An energetic muon can destroy a carbon nucleus in LS by spallation. Various radioactive isotopes and neutrons are generated by muon spallation. Table 1 shows a list of generated isotopes.

Spallation events due to muons are an important source of background. Most of the long life spallation products emit a single β-ray so they are eliminated by the delayed coincidence requirement. However ^{9}Li and ^{8}He produce both a β^- and neutron. For these we applied the following criteria to cut the correlated spallation events. (1) 2 ms veto is applied after any muon events. (2) Additional 2 s veto is applied for energetic muon events when the ionization energy

Table 1: Radioactive isotopes generated by muon spallation in the liquid scintillator.

Isotope	$T_{1/2}$	E_{max} (keV)
^{12}B	20.2 ms	13369 (β^-)
^{12}N	11.0 ms	17338 (β^+)
^{11}Li	8.5 ms	20610 (β^-)
^{9}Li	173.8 ms	13606 (β^-, n)
^{8}He	119.0 ms	10653 (β^-, n)
^{9}C	126.6 ms	16498 (β^+)
^{8}Li	838.0 ms	16006 (β^-)
^{6}He	906.7 ms	3508 (β^-)
^{8}B	770.0 ms	17979 (β^-)

deposit is larger than 10^6 p.e. ($\sim$3 GeV). (3) For smaller energy deposits (less than 10^6 p.e.) a 2 s veto is applied to events with vertices in a 3 m cylinder around the muon track.

Muon spallation in the rock surrounding the KamLAND detector can generate fast neutrons that penetrate through the water of outer detector. These fast neutrons can cause a correlated background since they can generate both prompt and delayed signal in the LS via a recoil proton and neutron capture γ-ray. Adopting a 5m radius fiducial volume eliminates most of this background.

Muon spallation provides not only background but also important calibration sources. Neutron captured on proton (2.2MeV γ), neutron captured on ^{12}C (4.9MeV γ) and ^{12}B decayed β are used for energy and vertex calibrations.

2 Result of Reactor $\bar{\nu}_e$ Observation

KamLAND is the first experiment to observe $\bar{\nu}_e$ disappearance from a reactor source. [1] In this section the reactor experiment analysis is described. The dominant background of reactor $\bar{\nu}_e$'s is geo-$\bar{\nu}_e$'s from β decay of U and Th in the earth. The geo-$\bar{\nu}_e$ flux has a expected energy distribution from 1 MeV to 2.4 MeV. [3] Since the total flux of geo-$\bar{\nu}_e$'s has large uncertainty, we applied an analysis energy threshold at 2.6 MeV for the reactor analysis.

2.1 $\bar{\nu}_e$ Flux from Reactors

Nuclear reactor power plants are strong electron anti-neutrino source. $\bar{\nu}_e$'s are generated by β decay of daughter nuclei from the fission of various fuel components, such as ^{235}U, ^{238}U, ^{239}Pu and ^{241}Pu. The flux of $\bar{\nu}_e$ from a reactor is calculated from the thermal power generation and the distance between the detector and reactor. The thermal power information is provided by the power companies with better than 2% accuracy. About 70GW (7% of the world total) of reactor power is generated at a distance of 175$\pm$35km from Kamioka. This corresponds to 80% of $\bar{\nu}_e$ flux at KamLAND. Fortunately this distance is suitable to observe LMA neutrino oscillation. In our data set of 145.1 live days, the expected number of reactor $\bar{\nu}_e$ events in the fiducial volume was 86 $\pm$ 5.6 events. The systematic uncertainties for reactor $\bar{\nu}_e$ detection are listed in the table 2.

2.2 Event Selection for Reactor $\bar{\nu}_e$

The selection criteria for $\bar{\nu}_e$ events is (1) total charge cut, less than 10,000 p.e. ($\sim$30MeV) with no OD veto signal and muon spallation cut. (2) fiducial volume cut ($R < 5$m), (3) time

Table 2: Systematic uncertainties of reactor $\bar{\nu}_e$ (%).

Total LS mass	2.1	Reactor power	2.0
Fiducial mass ratio	4.1	Fuel composition	1.0
Energy threshold	2.1	Time lag of β decay	0.28
Efficiency of cuts	2.1	ν spectra	2.5
Live time	0.07	Cross section	0.2
Total systematic error			6.4

correlation cut (0.5μs $< \Delta T < 660\mu$s), (4) vertex correlation cut ($\Delta R <$1.6m), (5) delayed energy window cut (1.8MeV $< E_{delay} <$ 2.6MeV), and (6) cut on the delayed vertex position more than 1.2m from central vertical axis to eliminate background from thermometers of LS.

After applying our cuts and a 2.6MeV analysis threshold, 54 events remained. The total background was estimated to be 0.95±0.99 events, where accidental background is 0.0086 ± 0.0005, background from ^{9}Li/^{8}He is 0.94 ± 0.85 and fast neutron is less than 0.5 events. The ratio of the number of observed reactor $\bar{\nu}_e$ events to expected events without oscillation is

$$\frac{N_{obs} - N_{BG}}{N_{expected}} = 0.611 \pm 0.085(\text{stat}) \pm 0.041(\text{syst}). \tag{4}$$

This result indicates $\bar{\nu}_e$ disappearance with 99.95% C.L.

2.3 Interpretation with Neutrino Oscillation

Neutrino oscillation is one of the most probable explanations to understand the observed deficit of $\bar{\nu}_e$'s. A "Rate analysis" was performed where oscillation parameters are examined by defining a χ^2,

$$\chi_{rate}^2 = \frac{(0.611 - R(\sin^2 2\theta, \Delta m^2))^2}{0.085^2 + 0.041^2} \tag{5}$$

where, $R(\sin^2 2\theta, \Delta m^2)$ is the ratio of expected number of events with oscillation to expected number of events without oscillation. Also a "Shape analysis", comparing the normalized energy spectrum of $\bar{\nu}_e$ was performed. Figure 1 shows the visible energy spectrum of the prompt signal that corresponds to the $\bar{\nu}_e$ spectrum. The upper figure is the expected reactor $\bar{\nu}_e$ energy spectrum with contributions from geo-$\bar{\nu}_e$ (model Ia)[3] and accidental background. The lower figure shows the energy spectrum of the observed prompt events (solid circles with error bars), along with the expected no oscillation spectrum (upper histogram, with geo-$\bar{\nu}_e$ and accidentals shown) and best fit (lower histogram) including neutrino oscillations. The shaded band indicates the systematic error in the best-fit spectrum. The vertical dashed line corresponds to the analysis threshold at 2.6MeV.

A maximum likelihood function was used to define the combined χ^2 of the rate and shape analysis.

$$\chi_{rate+shape}^2 = \chi_{rate}^2 + \chi_{BG}^2(N_{BG1\sim2}) + \chi_{dist}^2(\alpha_{1\sim4}) - 2\log L_{shape}(\sin^2\theta, \Delta m^2, N_{BG1\sim2}, \alpha_{1\sim4}) \tag{6}$$

where L_{shape} is the likelihood function of the spectrum including deformations from various parameters. $N_{BG1\sim2}$ are the estimated number of ^{9}Li and ^{8}He backgrounds and $\alpha_{1\sim4}$ are the parameters for the shape deformation coming from the energy scale, resolution, $\bar{\nu}_e$ spectrum and fiducial volume.

Figure 2 shows the neutrino oscillation parameter region for two neutrino mixing at the 95% C.L. The excluded region from Chooz[4] and Palo Verde[5] are shown at the top region. The allowed region of the LMA solution from solar neutrino experiments[6] is shown in the

middle region. The KamLAND "Rate" analysis excluded most of the region except LMA. The allowed region of LMA is split into two regions by the KamLAND "Rate+Shape" analysis. The remaining lower region is called LMA-1 and upper one is called LMA-2.
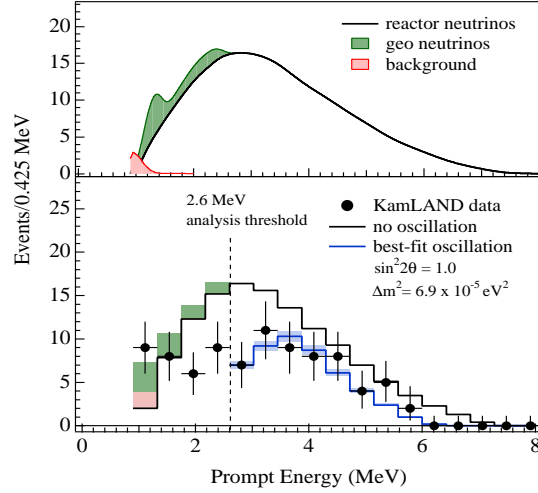

Figure 1: Expected $\bar{\nu}_e$ spectrum from the reactor (upper) and visible energy spectrum of the prompt signal (lower).
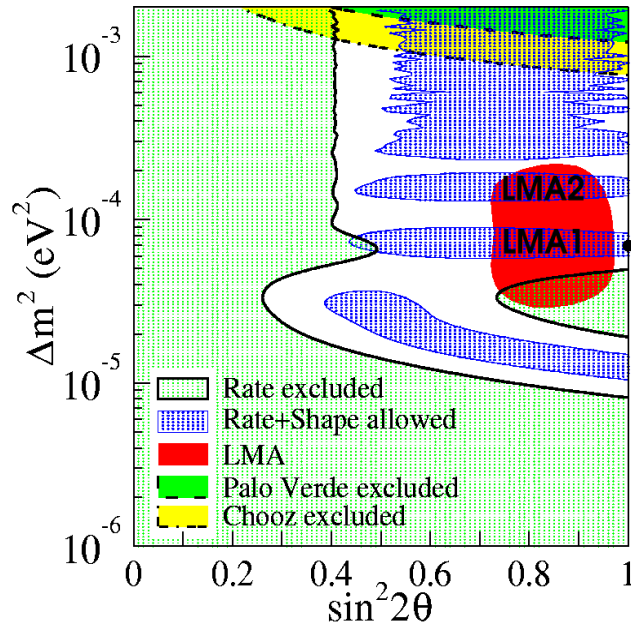

Figure 2: Neutrino oscillation parameters excluded by Chooz, Palo Verde, KamLAND (Rate) and allowed by solar-ν combined (LMA), KamLAND (Rate+Shape). Two regions (LMA-1, LMA-2) remain at 95%.C.L.

2.4   Future Prospects of the KamLAND Reactor $\bar{\nu}_e$ Observation

KamLAND is taking data continuously and an update on the reactor $\bar{\nu}_e$ analysis will be coming soon. The expected $\bar{\nu}_e$ flux is changing because some reactor power plants have shutdown for maintenance from September 2002. Figure 3 shows the time variation of the expected $\bar{\nu}_e$ flux from reactors and the observed number of $\bar{\nu}_e$ events at KamLAND. It is expected that a flux modulation analysis will check the consistency of the reactor $\bar{\nu}_e$ deficit. From 2006 another strong reactor "Shika2" located 88km from KamLAND will begin operation. Figure 4 shows the contribution to the $\bar{\nu}_e$ spectrum from "Shika2" considering the neutrino oscillation solutions

LMA-1 and LMA-2. Since the distance 88km is the most sensitive region to distinguish LMA-1 and LMA-2, it is expected that spectrum shape analysis will exclude one of these two solutions.
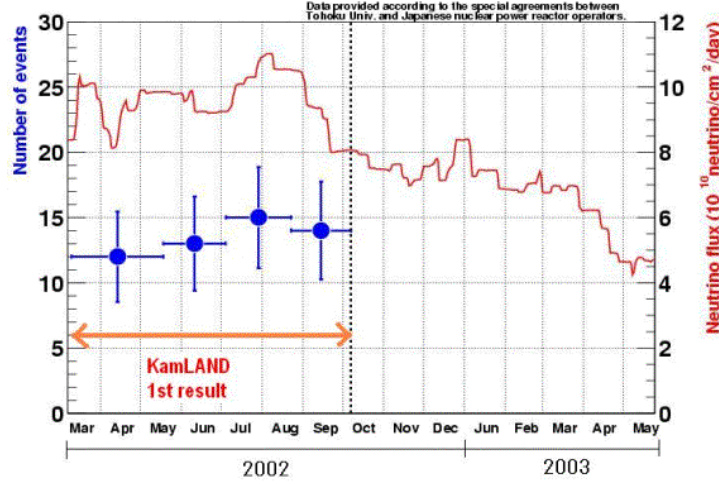

Figure 3: Time variation of the expected reactor $\bar{\nu}_e$ flux at KamLAND is shown (solid line). The observed number of reactor $\bar{\nu}_e$ events is also shown (solid circles with error bars).
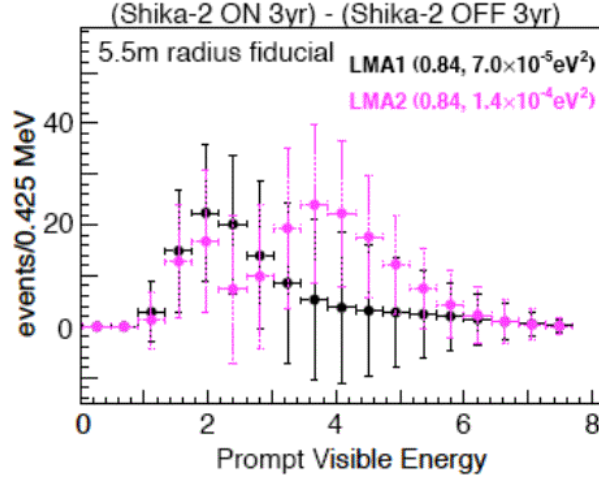

Figure 4: Expected $\bar{\nu}_e$ spectrum from the new reactor "Shika2" after 3 years exposure, considering the neutrino oscillation solutions LMA-1 and LMA-2.

3   Result of Solar $\bar{\nu}_e$ Search

Although neutrino oscillation is the most favored solution to explain the solar neutrino deficit other possible solutions are not completely excluded. The search for solar $\bar{\nu}_e$ [2,7] is an effective test to examine other exotic solutions. In this section an analysis of 185.5 live days KamLAND data is discussed.

3.1   Possible Mechanisms to Allow the Solar $\bar{\nu}_e$

It is generally believed that neutrinos from the Sun are generated by fusion of light nuclei (mainly protons) in the core. Anti neutrinos are not generated among the many processes of the fusion in the Sun, so we should assume some other mechanism to produce solar $\bar{\nu}_e$. In this letter two models are discussed. The first is a hybrid model [8] of resident spin flavor precession (RSFP) and the Mikheyev-Smirnov-Wolfenstein (MSW) effect. In this model ν_e with non-zero transition magnetic moment can evolve into $\bar{\nu}_\mu$ or $\bar{\nu}_\tau$ while propagating through intense magnetic fields in the solar core and they can in turn evolve into $\bar{\nu}_e$ via the MSW effect. The other mechanism

comes from a model of neutrino decay[9], where a heavy neutrino mass eigenstate may decay into a lighter anti-neutrino mass eigenstate.

3.2 Event Selection for Solar $\bar{\nu}_e$

The dominant component of solar ν_e flux above the current KamLAND analysis threshold (2.6MeV) is the ^{8}B neutrino flux, which extends up to 14 MeV. The reactor $\bar{\nu}_e$'s, who's energies extend up to 7 MeV, become a source of background events for the solar $\bar{\nu}_e$ analysis. Figure 5 shows expected visible energy spectrum of the reactor $\bar{\nu}_e$ together with the $\bar{\nu}_e$ spectrum from ^{8}B neutrino assuming that 1% of flux is converted from ν_e to $\bar{\nu}_e$. The lower analysis threshold (7.5MeV) corresponds to the end point of reactor $\bar{\nu}_e$ spectrum and upper one (14.0MeV) corresponds to that of the ^{8}B ν_e spectrum. The criteria to select solar $\bar{\nu}_e$ events is (1) total charge cut, less than 10,000 p.e. ($\sim$30MeV) with no OD veto signal and muon spallation cut. (2) fiducial volume cut ($R < 5.5$m), (3) time correlation cut (0.5μs $< \Delta T < 660\mu$s), (4) vertex correlation cut ($\Delta R <$1.6m), (5) delayed energy window cut (1.8MeV $< E_{delay} <$ 2.6MeV), (6) LS thermometer cut, and finally (7) prompt energy cut for solar $\bar{\nu}_e$ (7.5MeV $< E_{prompt} <$ 14.0MeV). Data from 185.5 live days were included in this analysis. Figure 6 shows the prompt and delayed energy distribution of the candidate events before cut (7). After cut (7) no events remained. The total expected background was estimated to be 1.1$\pm$0.4 events, composing the backgrounds from reactor $\bar{\nu}_e$ (0.2$\pm$0.2), atmospheric ν (0.001), fast neutrons (0.3$\pm$0.2), accidental coincidences (0.02) and ^{8}He/^{9}Li (0.6$\pm$0.2). Systematic uncertainties are summarized in Table 3.

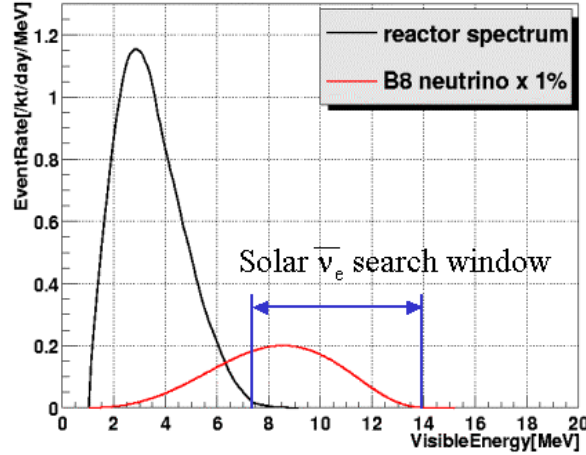Figure 5: Expected visible energy spectrum of reactor $\bar{\nu}_e$ together with the $\bar{\nu}_e$ spectrum from ^{8}B neutrino assuming that 1% of flux is converted from ν_e to $\bar{\nu}_e$. The analysis energy range of solar $\bar{\nu}_e$ was 7.5MeV$< E_{prompt} <$14.0MeV.

Table 3: Systematic uncertainties of solar $\bar{\nu}_e$ (%).

Detection Efficiency	1.6	Cross section	0.2
Number of target protons	4.3	Energy threshold	4.3
Live time	0.07		
Total systematic error			6.3

3.3 Upper Limit of Solar $\bar{\nu}_e$ Flux

Since no candidates are found in the corresponding energy region, the upper limit of solar $\bar{\nu}_e$ flux is calculated using the Feldman-Cousins method[10] with $\bar{\nu}_e$ cross section ($\sigma = 6.88 \times 10^{-42}$cm^2), detection efficiency ($\varepsilon = 0.841$), live time ($T = 1.60 \times 10^7$s) and number of target protons ($\rho_p \times f_v = 4.61 \times 10^{31}$). At the 90% C.L. the upper limit of solar $\bar{\nu}_e$ flux is $\phi_{\bar{\nu}_e} < 3.7 \times 10^2$
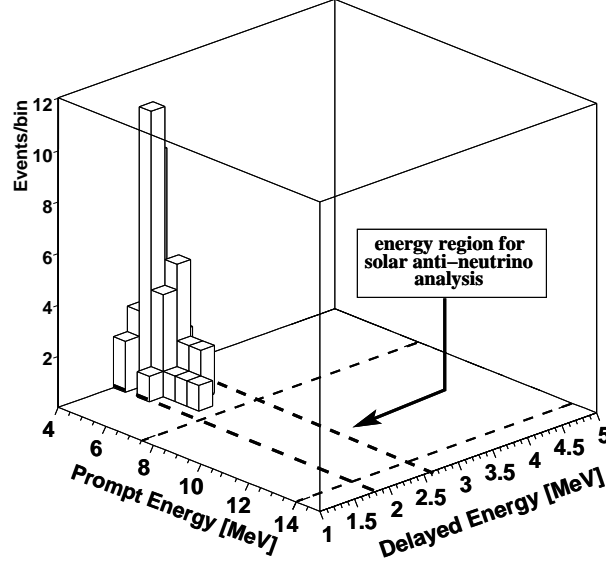
Figure 6: Prompt and delayed energy distribution from the solar $\bar{\nu}_e$ candidates before the final energy cut (7) (see text). No events remained in the energy range 7.5MeV< E_{prompt} <14.0MeV and 1.8MeV< E_{delay} <2.6MeV.

cm^{-2}s^{-1}. Since 29.5% of total ^{8}B neutrino flux of $5.05^{+1.01}_{-0.81} \times 10^6$cm^{-2}s^{-1} is contained within the energy window of this analysis, the ν_e to $\bar{\nu}_e$ conversion probability without neutrino oscillation is 2.8×10^{-4} at 90% C.L. If we assume this conversion occurs by RSFP+MSW[8] and also assume the recent best fit of oscillation parameters [11] ($\sin^2 \theta = 0.28, \Delta m^2 = 7.2 \times 10^{-5}$eV^2), and a solar magnetic field model [12], the upper limit of the neutrino transition magnetic moment μ_ν and magnetic field B_{max} is estimated as $\mu_\nu \cdot B_{max} < 1.4 \times 10^{-5} \mu_B G$ (90%C.L.). If we assume neutrino decay,[9] we can constrain the lifetime limit to $\tau_2/m_2 > 6.7 \times 10^{-2}$ s/eV.

4 Summary

KamLAND has observed an evidence for the reactor $\bar{\nu}_e$ disappearance at 99.95% C.L. Assuming CPT invariance only the LMA solution is compatible with the deficit. We got an upper limit of the solar ν_e to $\bar{\nu}_e$ conversion probability 2.8×10^{-4} at 90% C.L. in the energy range 8.3MeV $< E_{\bar{\nu}_e}$ 14.8MeV. The KamLAND experiment is supported by the COE program of the Japanese Ministry of Education, Culture, Sports, Science, and Technology and the United States Department of Energy.

References

1. K. Eguchi *et al.* (KamLAND Collaboration), *Phys. Rev. Lett.* **90**, 021802 (2003).
2. K. Eguchi *et al.* (KamLAND Collaboration), *Phys. Rev. Lett.* **92**, 071301 (2004).
3. R. S. Raghavan *et al.*, *Phys. Rev. Lett.* **80**, 635 (1998).
4. M. Apollonio *et al.*, *Phys. Lett.* B **466**, 415 (1999).
5. F. Boehm *et al.*, *Phys. Rev.* D **64**, 112001 (2001).
6. G. L. Fogli *et al.*, *Phys. Rev.* D **66**, 053010 (2001).
7. H. Ogawa, PhD Thesis "Search for Electron Anti-Neutrinos from the Sun using the KamLAND Large Volume Liquid Scintillator Detector", 2003.
8. C. S. Lim *et al.*, *Phys. Lett.* B **243**, 389 (1990); R. S. Raghavan *et al.*, *Phys. Rev.* D **44**, 3786 (1991); E. Kh. Akhmedov and J. Pulido, *Phys. Lett.* B **553**, 7 (2003).
9. A. Acker *et al.*, *Phys. Lett.* B **285**, 371 (1992).
10. G. J. Feldman and R. D. Cousins, *Phys. Rev.* D **57**, 3873 (1998).
11. M. Nakahata, International Workshop on Neutrino Oscillations and their Origin, 2004.
12. H. M. Antia *et al.*, astro-ph/0005587.